/

Article / Book Information

Title	Enhancement of Stimulated Raman Scattering in Terrace-Microspheres
Authors	Hiyori Uehara, Tetsuo Kishi, Tetsuji Yano, Shuichi Shibata
Citation	Journal of the Optical Society of America B, Vol. 28, No. 10, p. 2436-2443
Pub. date	2011, 9
Copyright	Copyright (c) 2011 Optical Society of Americ

Enhancement of stimulated Raman scattering in terrace-microspheres

Hiyori Uehara,* Tetsuo Kishi, Tetsuji Yano, and Shuichi Shibata

Department of Chemistry and Materials Science, Tokyo Institute of Technology,
2-12-1 Ookayama, Meguro-ku, Tokyo, 152-8550, Japan
*Corresponding author: hiyori@glass.ceram.titech.ac.jp

Terrace-microspheres of high-index glass (BaO-SiO$_2$-TiO$_2$ glass, $n_D = 1.93$) containing 0.3 ppm of Nd^{3+} were used to investigate the interaction between Raman scattering due to a glass matrix and fluorescence due to Nd^{3+}. The terrace-microspheres were pumped with a tunable CW Ti:sapphire laser (790 nm–830 nm wavelength) for changing pumping wavelengths. With pumping in the 800–830 nm wavelength region, there was a spectral overlap between Raman scattering and Nd^{3+} fluorescence. Under such conditions, Nd^{3+} fluorescence works as a seeding and an amplifier of stimulated Raman scattering (SRS), resulting in SRS enhancement. With pumping of 20 mW power at around 830 nm wavelength, the terrace-microspheres showed the strongest SRS gain, 5–6 times of that of 790 nm wavelength pumping. SRS thresholds of the terrace-microspheres were improved from 3 mW (790 nm wavelength pumping) to 0.3 mW (830 nm pumping) due to the enhancement effect. The potential application for a multiwavelength Raman laser with a low threshold was demonstrated in the near-IR region ($\lambda = 840$–940 nm).   © 2011 Optical Society of America

OCIS codes: 140.3945, 160.5690, 180.5655, 190.5650, 290.5910, 300.6450.

1. INTRODUCTION

Stimulated Raman scattering (SRS) is an important nonlinear optical effect for generating tunable coherent radiation. Glasses are particularly attractive as the materials for Raman resonators because their broad gain bandwidths enable us to achieve high tunability of emission wavelengths. In optical fibers, due to the low optical losses of silica-glass-based optical fibers and broad Raman bandwidths, the development of various types of Raman fiber lasers has been reported [1].

Microcavity-based Raman lasers are also highly attractive for extending the available wavelength of the existing laser source. In high-quality (high-Q) microspheres, their whispering gallery modes (WGMs) enhance Raman gains compared with those of bulk samples. Recently, low-threshold spherical Raman lasers were demonstrated with high-Q silica glass microspheres and silica glass toroids several tens of micrometers in diameter using a fiber-taper optical coupler [2,3]. A low-threshold Raman laser was also demonstrated with CaF$_2$ crystalline resonators using angle-polished fiber [4]. Glass microspheres are expected to have potential uses such as light sources of multiwavelengths [5] and low-threshold microlasers [6]. To excite high-Q silica microspheres (refractive index $n_D = 1.45$), highly effective optical coupling of pumping light into them is inevitable. Various techniques for achieving sufficient optical coupling with silica glass spheres have been tried using prism couplers [7], side-polished fibers [8], fiber tapers [9], and so on. Among these coupling techniques, the fiber tapers with few-micrometer diameters showed remarkable optical coupling efficiency. Silica glass spheres should be pumped with silica glass fiber taper to match the refractive index and modes between the microspheres and the fiber tapers. Fiber tapers, however, are drawn delicately from silica-based optical fibers, and from a practical viewpoint, fiber tapers with few-micrometer diameters are very fragile.

Thus, the development of other optical coupling techniques is an urgent issue.

Glass microspheres of multicomponent glasses such as those made from conventional optical glasses are also attractive because of the wide variety of compositions along with their wide range of optical and physical properties. Optical coupling using silica-glass-based fiber taper is not suitable for pumping those multicomponent glass spheres, because their refractive-index difference does not allow mode matching. Therefore, an efficient coupling technique to the multicomponent glass spheres is required for practical devices.

In our previous work, a micrometer-sized spherical cavity laser having a terrace-shaped pumping light entrance was investigated [10–12]. A terrace portion was formed on microspheres of multicomponent glasses ($n_D = 1.93$) several tens of micrometers in diameter using organic–inorganic hybrid materials ($n_D = 1.45$) in the binary system of 3-methacryloxypropyltrimethoxysilane (MOPS) and tetramethoxysilane (TMOS). A microcapillary supplier of picoliter-volume sol was used for the terrace formation. We reported the mechanism of terrace formation and the suitable lasing conditions, including terrace thickness, for SRS [13]. Stimulated Raman emission of WGMs was demonstrated by pumping the spot at the terrace portion with a CW Ar+ laser (514.5 nm wavelength). A terrace-microsphere is useful for coupling with high-index spheres, and SRS has been demonstrated by just directly laser irradiating the terrace portion in a terrace-microsphere. Terrace-microspheres are one successful example of spherical lasers, and with a terrace entrance a wide variety of multicomponent glasses of high refractive index will be applicable in micrometer-sized optical resonators [14].

Since stimulated Raman emission builds up from spontaneous Raman scattering, usually relatively high pumping power is required for achieving notable conversion

efficiencies. Recently, many authors have tried to find new methods for enhancing SRS in gas and liquid mediums. Various external seeding techniques were applied to reduce the threshold of SRS: (1) fluorescence-seeded Raman generation, where the cells of Raman and dye are separated and the seeding beam for Raman cells (gaseous CH_4) was provided from a cell containing dye (Rhodamine 640) [15], (2) fluorescence seeding by dissolving fluorescent dye in an ethanol droplet [16], and (3) fluorescence working as an amplifier of SRS emission [Raman emission of CS_2 cells was amplified by passing through the fluorescent dye cell (Rhodamine 6G)] [17].

In this paper, terrace-microspheres consisting of high-index glass spheres (BaO-SiO$_2$-TiO$_2$ glass) containing Nd^{3+} were used to investigate the interaction between the double effects of Raman scattering due to a glass matrix and fluorescence due to Nd^{3+}. When pumping at longer wavelengths than 800 nm, there is a spectral overlap between Raman and fluorescence. Under such conditions, SRS and fluorescence cannot be treated independently, and enhancement of SRS is expected in terrace-microspheres by pumping with a tunable Ti:sapphire laser. This is the first report (to our knowledge) of SRS enhancement by fluorescence in the solid-state spherical cavity. Study of the interaction between SRS and rare-earth fluorescence in a glass matrix is attractive both scientifically and technologically. Terrace-microspheres consisting of Nd^{3+}-doped high-index glass spheres will open a way to develop a spherical Raman laser with a low-threshold multiwavelength emission.

2. EXPERIMENTAL PROCEDURES

Commercially available high-refractive-index $(n_D = 1.93)$ glass microspheres 21 and 40 μm in diameter (Union Co.) were used for the fabrication of terrace-microspheres. Typical composition of the glass sphere is 38.0BaO-11.5SiO$_2$-38.5TiO$_2$-6.7CaO-5.3ZnO [18] in the BaO-SiO$_2$-TiO$_2$ glass system containing a small amount of Nd^{3+}. In order to estimate the concentration of Nd^{3+} in this glass, fluorescence at around 900 nm wavelength of a bulk glass was measured. The Nd^{3+} content in this glass was measured as about 0.3 ppm by comparing the fluorescent intensity of the high-index glass with that of the standard Nd^{3+}-doped glasses (soda-lime silicate glass). Microspheres were made by the flame spray technique, where small pieces of glass cullet were melted in the flame and smooth-surface glass spheres were formed by their surface tension. Organic–inorganic hybrid materials were prepared by the sol-gel technique using MOP) and TMOS as starting materials. MOPS and TMOS were chosen to control the sol characteristics, such as hydrophobic–hydrophilic properties, viscosity, and polymerization rate. The 25MOPS–75TMOS sol in the MOPS–TMOS binary system was hydrolyzed and polymerized in hydrochloric acid solution at room temperature. Relative humidity of the atmosphere was controlled below 15% in a dry box. Using capillary-puller equipment, glass microcapillaries of about 1 μm tip diameter were prepared in advance. A picoliter of MOPS–TMOS sol was supplied by the microcapillary into the extremely narrow space between a sphere and a Teflon sheet [13]. A sol droplet with a volume of 1 pL was supplied in the narrow space by the capillary. While a glass sphere sank slightly into the sol, the sol solidified rapidly. After gelling, terrace-microspheres were dried at room temperature, then subsequently heated at 100 °C for 60 min.

As a preliminary measurement, spontaneous Raman scattering spectra of the BaO-SiO$_2$-TiO$_2$ and SiO$_2$ glasses were measured by a microscopic Raman scattering spectrometer (JASCO, Model NRS-2100). The pumping wavelength was 514.5 nm (CW Ar$^+$ laser), with a spectral resolution of 1 cm^{-1}. The incident laser beam was collimated to about a 1 μm diameter spot.

Moreover, the fluorescence spectrum and the excitation spectrum of the Nd^{3+}-doped BaO-SiO$_2$-TiO$_2$ glass were measured by pumping with a tunable CW Ti:sapphire laser (pumping wavelength λ_{pump} = 780 nm–830 nm). A schematic of the setup for the pumping experiments is shown in Fig. 1.
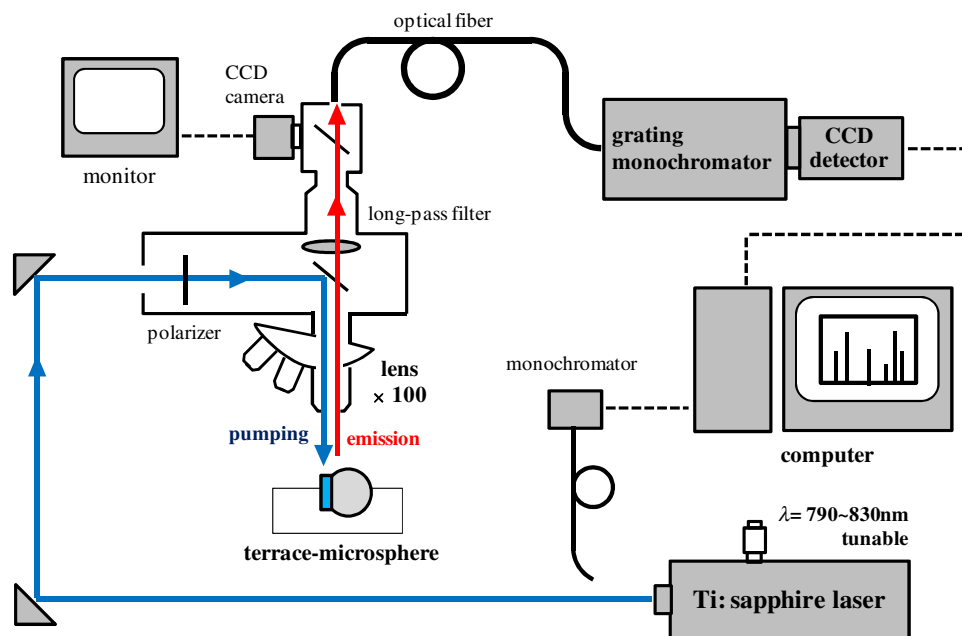

Fig. 1.   (Color online) Schematic illustration of setup for pumping terrace-microspheres.

A tunable CW Ti:sapphire laser ($\lambda_{pump} = 790\,nm$–$830\,nm$) was used for changing pumping wavelengths. The incident laser beam was collimated to about a $2\,\mu m$ diameter spot by an objective lens ($\times 100$, NA0.8). Terrace-microspheres were fixed on the edge of a slide glass by an electrostatic force, and the terrace portion was directly pumped by the laser light spot. A long-pass filter was used to remove emissions at shorter wavelengths than $835\,nm$. The emissions from the terrace-microspheres were sent to a grating monochromator (JASCO, CT-25C) through an optical fiber and analyzed by a CCD detector (ANDOR, iDus DU401A). Pumping wavelengths (λ_{pump}) were monitored by a monochromator (OceanOptics, USB4000). Pumping powers at the sample position were measured by a laser power meter (OPHIR, PD300-3W). To investigate the interaction between SRS and Nd^{3+} fluorescence, various emission spectra of the terrace-microspheres were measured by changing the pumping wavelength from $790\,nm$ to $830\,nm$. Subsequently, emission intensities were plotted against the pumping power, and SRS thresholds were estimated at various pumping wavelengths.

3. RESULTS AND DISCUSSION

Figure 2(a) shows a typical SEM image of the terrace-microspheres. A terrace was successfully formed on a glass sphere. Typical sizes of terrace-microspheres are illustrated in Fig. 2(b): a glass sphere $21\,\mu m$ in diameter, with a terrace portion $16\,\mu m$ in diameter and $4\,\mu m$ in height. In the pumping experiments, glass spheres of different diameters were used: 21 and $40\,\mu m$. The refractive index of the 25MOPS-75TMOS hybrid material was $n_D = 1.45$ after curing.

High-index BaO-SiO_2-TiO_2 glass spheres containing $0.3\,ppm$ of Nd^{3+} were used in the pumping experiments. Spontaneous Raman scattering spectra of BaO-SiO_2-TiO_2 and silica glasses are shown in Fig. 3. High-index BaO-SiO_2-TiO_2 glass showed strong Raman scattering in wide range of wavelengths compared with that of the silica glass. In the BaO-SiO_2-TiO_2 glass, peaks at 300 and $800\,cm^{-1}$ originated from bonds of Ti-O and Si-O in the BaO-SiO_2-TiO_2 glass matrix [19,20]. The intensity of Raman scattering of high-index glass (at $800\,cm^{-1}$

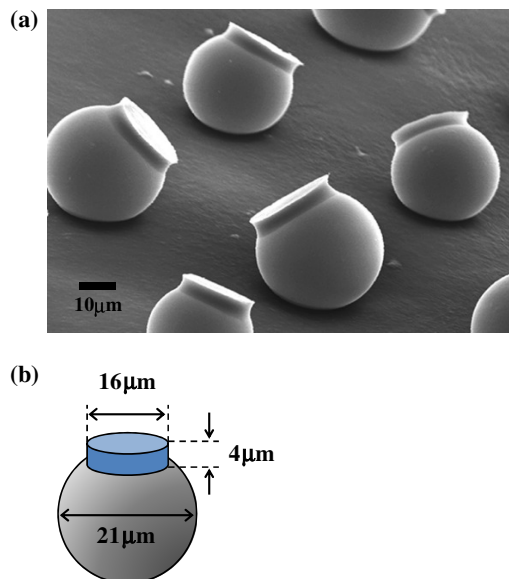**(a)**

(b)

16μm

4μm

21μm

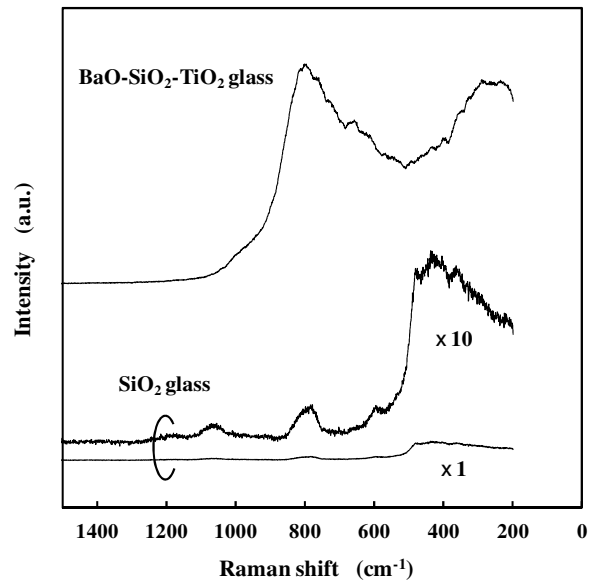Fig. 2.   (Color online) (a) SEM image of terrace-microspheres, (b) schematic illustration of a terrace-microsphere.

Fig. 3.   Spontaneous Raman scattering spectra of BaO-SiO_2-TiO_2 and SiO_2 glasses.

Raman shift) was about 11 times larger than that of SiO_2 glass (at $430\,cm^{-1}$ Raman shift). Since the BaO-SiO_2-TiO_2 high-index glass showed strong Raman scattering in wide range of wavelengths compared with that of the silica glass, a multi-component glass is one of the most favorable candidates for multiwavelength Raman lasers.

The BaO-SiO_2-TiO_2 glass microspheres also contained $0.3\,ppm$ of Nd^{3+}, which is a well-known active ion for laser emission [21,22]. In Fig. 4, fluorescence and excitation spectra of Nd^{3+}-doped BaO-SiO_2-TiO_2 bulk glass are shown. The fluorescence was obtained by pumping the sample at a $810\,nm$ wavelength. The excitation spectrum was measured by monitoring the fluorescence peak at $880\,nm$ wavelength. The excitation and fluorescent spectra showed the maximum at around 810 and $883\,nm$ wavelengths, respectively. Pumping by laser light at around a $810\,nm$ wavelength (the transition $^4I_{9/2} - {}^4F_{5/2}$) gave three principal fluorescent bands (wavelengths: 880, 1060, and $1325\,nm$). Transition $^4I_{3/2} - {}^4I_{9/2}$ gave fluorescence in the 860–$940\,nm$ wavelength, as shown in Fig. 4. When pumping the Nd^{3+}-doped BaO-SiO_2-TiO_2 glass at longer wavelengths than $800\,nm$, there would be a spectral overlap between Raman and fluorescence. Under such conditions, SRS enhancement is expected in terrace-microspheres by pumping with a tunable Ti:sapphire laser.
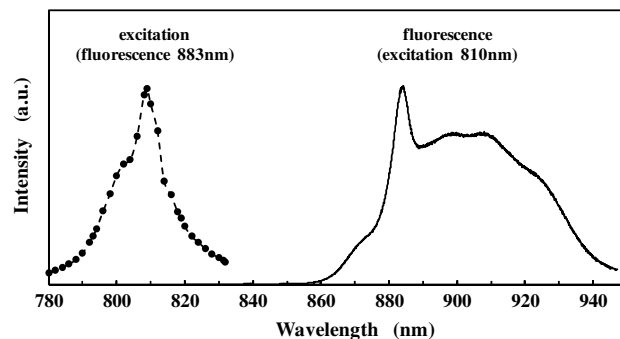

Fig. 4.   Fluorescence and excitation spectra of Nd^{3+}-doped BaO-SiO_2-TiO_2 glass.

Emission spectra of terrace-microspheres $21\,\mu m$ in diameter pumped with various wavelengths are shown in Fig. 5: 5(a) 792.7 nm, 5(b) 808.4 nm, 5(c) 819.3 nm, and 5(d) 830.2 nm. Pumping power was 20 mW. In the same figure, to make the origin of the emission spectra clear, Raman scattering and Nd^{3+} fluorescence bands were also plotted with blue and red dotted lines, respectively. The blue dotted lines show spontaneous Raman scattering spectra at the corresponding pumping wavelengths (using the data of the Raman spectrum
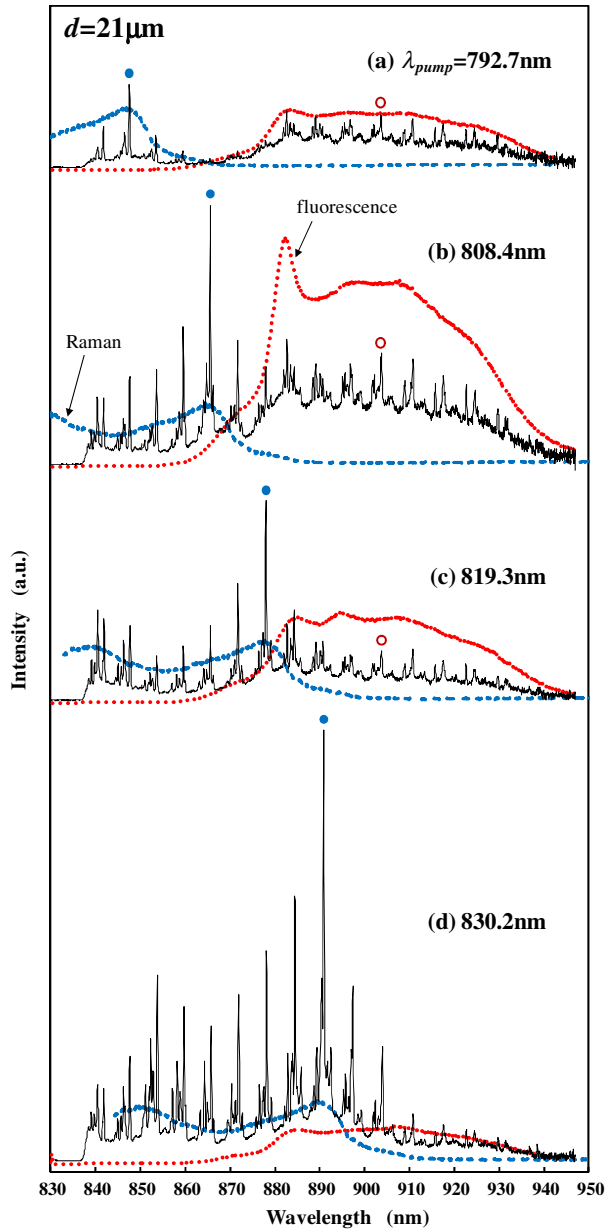

Fig. 5. (Color online) Emission spectra of a terrace-microsphere $21\,\mu m$ in diameter at various pumping wavelengths: (a) 792.7 nm, (b) 808.4 nm, (c) 819.3 nm, and (d) 830.2 nm. Pumping power was 20 mW. To make the spectral overlapping of Raman scattering and fluorescence clear, spectra of spontaneous Raman scattering (using the data of the Raman spectrum in Fig. 3) and Nd^{3+} fluorescence of Nd^{3+}-doped BaO-SiO_2-TiO_2 glass are also plotted with blue and red dotted lines, respectively. The blue solid and red hollow circles show the peaks used for plotting in Fig. 7: the emission peaks due to SRS (Raman shift is around $815\,cm^{-1}$) and fluorescence ($\lambda = 903.6\,nm$), respectively.

in Fig. 3). The red dotted lines show fluorescent spectra of Nd^{3+}-doped BaO-SiO_2-TiO_2 bulk glass at the corresponding pumping wavelengths. Emission peaks due to WGMs were observed on the broad backgrounds of spontaneous Raman and Nd^{3+} fluorescence. Relatively strong SRS peaks corresponding to around $815\,cm^{-1}$ Raman shift were highlighted with closed blue circles in the Fig. 5 spectra. On the other hand, open red circles on the fluorescence peaks show the WGMs due to Nd^{3+} at the same wavelength. When the pumping wavelength was changed from 792.7 to 830.2 nm, Raman scattering shifted to the longer wavelength side, and the overlapping of Raman scattering and fluorescence bands increased. For example, in the spectrum in Fig. 5(a), pumping at a 792.7 nm wavelength, Raman and fluorescence bands were not overlapped. In Figs. 5(b) and 5(c), pumping at 808.4 and 819.3 nm wavelengths, both bands were partially overlapped. Finally, in the spectrum in Fig. 5(d), pumping at a 830.2 nm wavelength, strong overlapping was observed. It should be noted that the SRS peak intensities increased with the shifting pumping wavelengths from Fig. 5(a) to 5(d). In Fig. 5(d), the highlighted SRS peak intensity corresponding to $820\,cm^{-1}$ Raman shift was 5.5 times larger than that of Fig. 5(a).

Emission spectra of the terrace-microsphere $40\,\mu m$ in diameter were also measured, as shown in Fig. 6. Mode spacing values between two adjacent modes in Figs. 5 and 6 were $85\,cm^{-1}$ (7.0 nm) and $41\,cm^{-1}$ (3.4 nm), respectively, at around a 900 nm wavelength, which corresponded to the sphere diameters. Similarly, the intensity of highlighted SRS peak increased from Fig. 6(a) to 6(d) with the pumping wavelengths changing to the longer side, also increasing the spectral overlapping of Raman and fluorescence, and the strongest SRS was observed in Figure 6(d).

The mode spacing of WGM is theoretically estimated from the sphere radius r, the refractive index of the sphere n_1, and the index of the surrounding medium n_2. The mode spacing (wavenumber) of a spherical particle is given by [6]

$$\Delta = \frac{\tan^{-1}\sqrt{(n_1/n_2)^2 - 1}}{2\pi r n_2 \sqrt{(n_1/n_2)^2 - 1}}. \tag{1}$$

Typical mode spacing of the terrace-microspheres in Fig. 5 is $85\,cm^{-1}$ at around a 900 nm wavelength. In this terrace-microsphere (refractive index of the high-index sphere $n_1 = 1.93$, terrace portion $n_2 = 1.45$), mode spacing is theoretically estimated from Eq. (1) as $86\,cm^{-1}$. Thus the measured mode spacing in Fig. 5 agrees well with the theoretical value. Moreover, the mode spacing of the terrace-microspheres in Fig. 6 is $41\,cm^{-1}$ at around a 900 nm wavelength, which is similar to the theoretically estimated value of $45\,cm^{-1}$. Their Q-values were calculated from the FWHM of the spectrum as about 10^4 and were limited by the resolutions of the spectrometer and CCD detector.

In Fig. 7, emission intensities of a terrace-microsphere $21\,\mu m$ in diameter [the same sphere shown in Figs. 5(a)–5(d)] are plotted against the pumping power. The blue and red curves in Figs. 7(a)–7(d) correspond to the blue and red circles in Fig. 5 and show the resonant peaks due to SRS (around $815\,cm^{-1}$ Raman shift) and the fluorescence ($\lambda = 903.6\,nm$). In Fig. 7(d), the peak intensity at a 903.6 nm wavelength was not plotted because the emission seemed to originate from
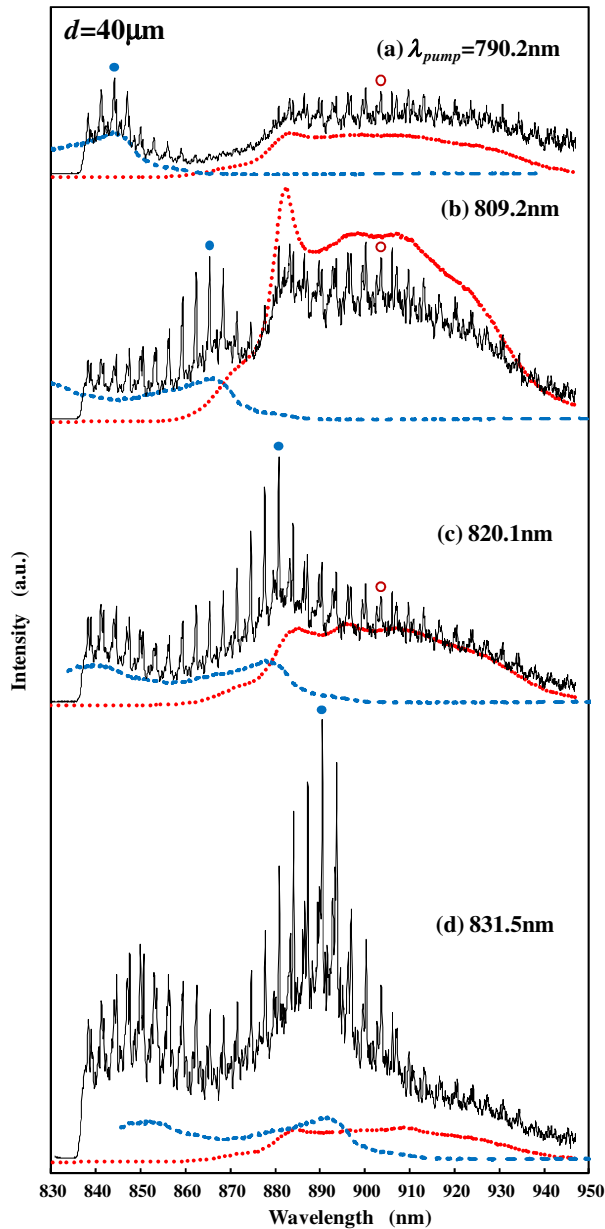
Fig. 6. (Color online) Emission spectra of a terrace-microsphere 40 μm in diameter at various pumping wavelengths: (a) 790.2 nm, (b) 809.2 nm, (c) 820.1 nm, and (d) 831.5 nm. Pumping power is 20 mW.

both Raman and fluorescence. The plots at low pumping powers are scaled up in the insets to make the threshold clear. In the SRS and Nd^{3+} fluorescence plots of Figs. 7(a)–7(d), the slopes of emission intensity versus pumping power increased clearly above thresholds. In the insets of Figs. 7(b) and 7(c), the change point of the slope in Nd^{3+} fluorescence intensity versus pumping power seemed to correlate with the threshold of SRS (1 and 0.6 mW, respectively). At a pumping power above the SRS threshold, the energy of Nd^{3+} fluorescence converted into SRS emissions, and the slope of the fluorescence curve decreased clearly. The slope of the SRS curve decreased at a high pumping power, as shown in Fig. 7, which was attributed to the gain saturation.

Thresholds of SRS and Nd^{3+} fluorescence of the terrace-microspheres at various pumping wavelengths are shown in
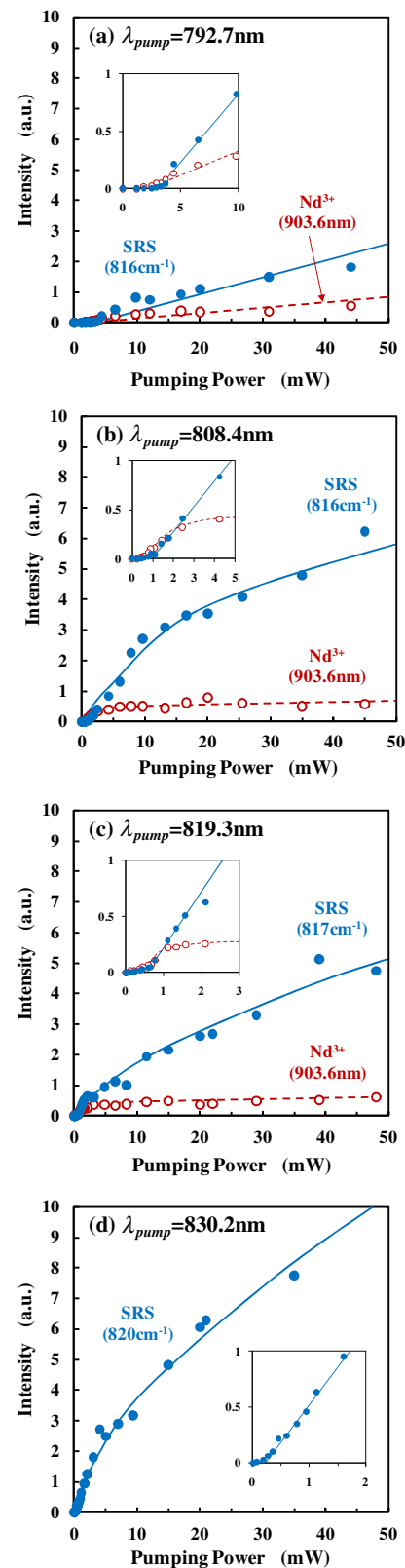

Fig. 7. (Color online) Emission intensities of a terrace-microsphere 21 μm in diameter (same sphere as shown in Fig. 5) were plotted against pumping power at various pumping wavelengths: (a) 792.7 nm, (b) 808.4 nm, (c) 819.3 nm and (d) 830.2 nm. The blue and red curves correspond to the blue and red circles in Fig. 5: the emission peaks due to SRS (Raman shift is around 815 cm^{-1}) and fluorescence ($\lambda = 903.6$ nm). The plots at low pumping powers are scaled up the insets to make the threshold clear.

Figs. 8(a) and 8(b). The SRS thresholds decreased from (a) to (d): (a) 3 mW, (b) 1 mW, (c) 0.6 mW and (d) 0.3 mW. On the other hand, as shown in Fig. 8(b), thresholds of emissions due to Nd^{3+} were 2.5–3 mW at around a 790 nm pumping wavelength and decreased drastically below 0.5 mW at longer wavelengths than 800 nm. With pumping at around a 820–830 nm wavelength, SRS with a threshold of 0.3 mW was performed in terrace-microspheres. This threshold is the best value for terrace-microspheres compared with our demonstration in the previous works (2.5 mW [8,11]). It should be noted that Nd^{3+} thresholds were always lower than those of the SRS at all pumping wavelengths [compare Figs. 8(a) and 8(b)].

Normalized SRS gains at a pumping power of 20 mW (estimated from the results in Figs. 5 and 6) are plotted against the pumping wavelength in Fig. 9. Closed and open circles correspond to the data of terrace-microspheres shown in Fig. 5 ($d = 21\,\mu$m) and Fig. 6 ($d = 40\,\mu$m), respectively. "Normalized SRS gain" is [strongest SRS peak intensities at various pumping wavelengths]/[SRS peak intensity at 816 cm^{-1} Raman shift at a 790 nm pumping wavelength]. With a shift in the pumping wavelength, normalized SRS gain increased. With pumping at around 830 nm, the terrace-microspheres showed the strongest SRS gain, which is 5–6 times of that of $\lambda_{\rm pump} \approx 790$ nm.

In this work, two emissions of SRS and fluorescence can traverse each emission center because both emissions are simultaneously generated from the same glass spheres by laser pumping. Therefore, SRS enhancement by fluorescence will cause both processes of seeding [15] and amplification [17]. Schematics of two Raman enhancement processes are shown in Fig. 10: 10(a) seeding, 10(b) amplification. Stokes frequency $\omega_s = \omega_{\rm pump} - \omega_{\rm vib}$, where $\omega_{\rm pump}$ is the frequency of the pumping laser and $\omega_{\rm vib}$ is a vibrational mode of the glass matrix. Seeding will be provided by not only spontaneous Raman scattering but also Nd^{3+} fluorescence when Raman and fluorescence bands overlap spectrally. Generally, for SRS without external seeding, SRS intensity I_s is given by the following equation [16,23]:

$$I_s = I_{sp} \times \exp(I_p g_s - \alpha)L, \qquad (2)$$

where I_{sp} is the intensity of the spontaneous Raman scattering, I_p is the pumping intensity, g_s is the Raman gain, α is absorption and scattering loss, and L is the optical path length in a microsphere. With seeding by fluorescence, the Stokes
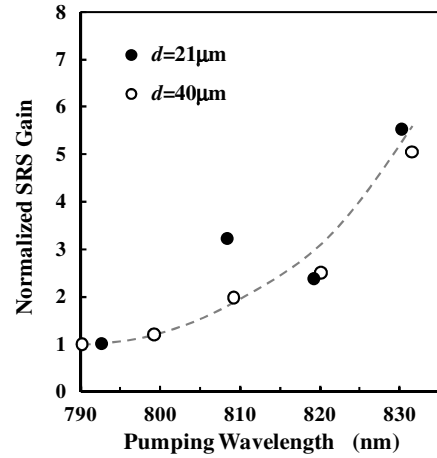
Fig. 9. Normalized SRS gain plotted against pumping wavelength (pumping power was 20 mW). Closed circles and open circles correspond to the terrace-microsphere shown in Fig. 5 ($d = 21\,\mu$m) and Fig. 6 ($d = 40\,\mu$m), respectively. Normalized SRS gain = [strongest SRS peak intensities at various pumping wavelengths] / [SRS peak intensity at 816 cm^{-1} Raman shift at 790 nm pumping wavelength].

emission no longer needs to start from spontaneous Raman scattering, but it can initiate from fluorescence spectrally overlapping the Raman band. Then SRS intensity becomes

$$I_s = [I_{sp} + I_f(\omega_s)] \times \exp(I_p g_s - \alpha)L, \qquad (3)$$

where $I_f(\omega_s)$ is the intensity of the fluorescence centered at ω_s (overlapping the Raman band) and is proportional to the product of the fluorescence cross section and the concentration of Nd^{3+}. I_{sp} is proportional to the product of the spontaneous Raman cross section. $I_f(\omega_s) > I_{sp}$ even at very low Nd^{3+} concentration, because the cross section of fluorescence is much larger than that of Raman scattering. Fluorescence seeding lowers the SRS threshold and enhances the SRS signal. Various methods such as external and internal seeding using lasing dye and liquid Raman medium for reducing the SRS threshold and enhancing the weaker gain of SRS were reported [15,16,23–25].

As shown in Fig. 10(b), the SRS amplification process by fluorescence was also observed. The Stokes emission (ω_s) from the glass matrix traverses the Nd^{3+} fluorescence medium (Nd^{3+} is under population inversion) and causes stimulated emission at the Stokes wavelength. The mechanism is similar to signal amplification in a rare-earth-ion-doped optical fiber. The power gain g is given by [17]

$$g \approx \exp\{(\sigma \Delta n_0 - \alpha)L\}, \qquad (4)$$

where σ is the cross section of the resonant absorption, Δn_0 is the initial density of inverted Nd^{3+}, and L is the optical path length in a microsphere. When the input SRS signal is strong, the growth rate decreases with the increase of input SRS intensity. This is a well-known "gain saturation" phenomenon [26]. Recently, besides addition of a lasing dye into the solvent [23], other methods using separated cells between the Raman and fluorescence medium [17] were reported for SRS amplification and spectral narrowing of SRS signal [27,28]. Moreover, SRS enhancement can also be explained by the energy conversion of Nd^{3+} fluorescence intensity to SRS emission by the amplification process [Fig. 10(b)].
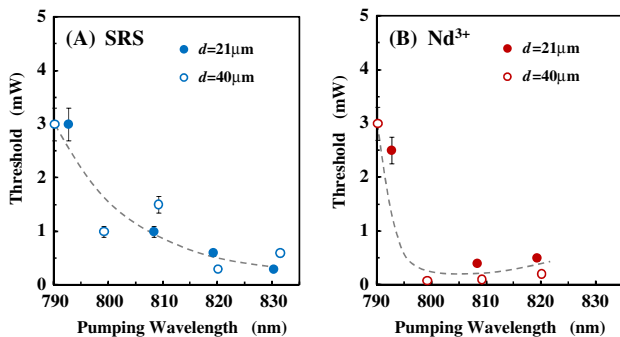

Fig. 8. (Color online) Thresholds of (a) SRS (Raman shift is around 815 cm^{-1}) and (b) Nd^{3+} emission at around 900 nm wavelength in the terrace-microspheres at various pumping wavelengths. Closed-circles and open-circles correspond to the terrace-microsphere shown in Fig. 5 ($d = 21\,\mu$m) and Fig. 6 ($d = 40\,\mu$m), respectively.
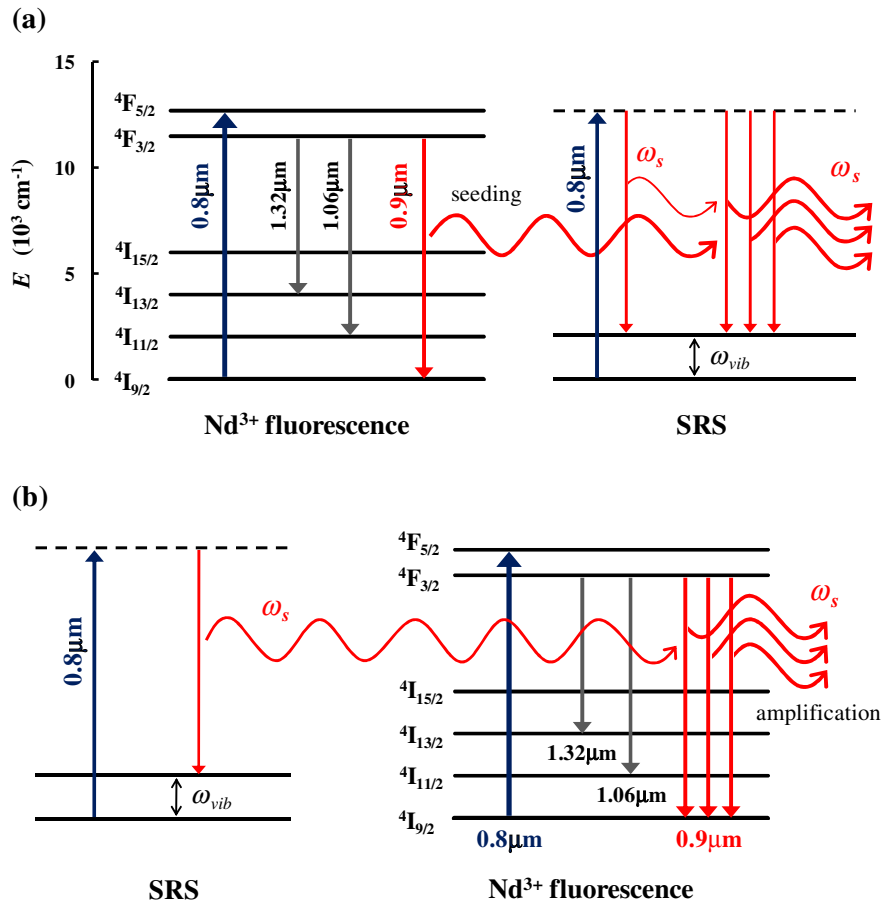
(a)

(b)

Fig. 10.   (Color online) Schematic diagrams of SRS enhancement by Nd^{3+} fluorescence. (a) Fluorescent seeding process for SRS, (b) SRS amplification process by fluorescence.

We also think the seeding [Eq. (3)] and amplification [Eq. (4)] were generated simultaneously and interacted with each other. However it is difficult to show a single model, because the seeding efficiency of amplified SRS and amplification efficiency of Nd^{3+}-seeded SRS (they depend on wavelength) are not clear at the present stage. Moreover, absorption of Nd^{3+} may also be related to the enhancement effect. We will attempt to measure the spectra at various Nd^{3+} concentrations to investigate the enhancement effect and influence of Nd^{3+} absorption in the future studies.

4. CONCLUSIONS

Terrace-microspheres consisting of high-index glass spheres (BaO-SiO$_2$-TiO$_2$ glass, $n_D = 1.93$) containing 0.3 ppm of Nd^{3+} were used to investigate the double effects of Raman scattering due to the glass matrix and fluorescence due to Nd^{3+}. The high-index glass showed strong Raman scattering in a wide range of wavelengths ($\sim 1000\,cm^{-1}$) compared with that of a silica glass. When pumping the Nd^{3+}-doped BaO-SiO$_2$-TiO$_2$ glass at longer wavelengths than 800 nm, there would be a spectral overlap between Raman and fluorescence. Terrace-microspheres of several tens of micrometers in diameter were pumped with a tunable CW Ti:sapphire laser at various pumping wavelengths ($\lambda = 790\,nm$–$830\,nm$) to control the overlap. Raman and fluorescence bands were not overlapped at $\lambda_{pump} \approx 790\,nm$. Pumping at the 800–830 nm wavelength region, there was a spectral overlap between Raman and fluorescence, and enhancement of SRS by Nd^{3+} fluorescence was

demonstrated. SRS thresholds of the terrace-microspheres were improved from 3 mW ($\lambda_{pump} \approx 790\,nm$) to 0.3 mW ($\lambda_{pump} \approx 830\,nm$) because of the enhancement effect. Pumping at around 830 nm, the terrace-microspheres showed the strongest SRS gain, which was 5–6 times of that of $\lambda_{pump} \approx 790\,nm$. In this work, two emissions of SRS and fluorescence can traverse each emission center because both emissions are simultaneously generated from the same glass spheres by laser pumping. Therefore, enhancement of SRS by fluorescence was caused by the two processes of "seeding" and "amplification" simultaneously in the terrace-microspheres. This is the first report of SRS enhancement by fluorescence in the solid-state spherical cavity. Terrace-microspheres consisting of Nd^{3+}-doped high-index glass spheres will open a way to develop a low-threshold spherical Raman laser for multiwavelength emission in the near-IR region ($\lambda = 840$–$940\,nm$).

REFERENCES

1. R. H. Stolen, "Fiber Raman lasers," Fiber Integr. Opt. **3**, 21–52 (1980).
2. S. M. Spillane, T. J. Kippenberg, and K. J. Vahala, "Ultralow-threshold Raman laser using a spherical dielectric microcavity," Nature **415**, 621–623 (2002).
3. T. J. Kippenberg, S. M. Spillane, D. K. Armani, and K. J. Vahala, "Ultralow-threshold microcavity Raman laser on a microelectronic chip," Opt. Lett. **29**, 1224–1226 (2004).
4. I. S. Grudinin and L. Maleki, "Efficient Raman laser based on a CaF$_2$ resonator," J. Opt. Soc. Am. B **25**, 594–598 (2008).

5. T. J. Kippenberg, S. M. Spillane, D. K. Armani, B. Min, L. Yang, and K. J. Vahala, "Fabrication, coupling and nonlinear optics of ultra-high-Q micro-sphere and chip-based toroid microcavities," in *Optical Microcavities*, K. J. Vahala, ed. (World Scientific, 2004), pp. 177–238.

6. P. W. Barber and R. K. Chang, *Optical Effects Associated with Small Particles* (World Scientific, 1988).

7. M. L. Gorodetsky, A. A. Savchenkov, and V. S. Ilchenko, "Ultimate Q of optical microsphere resonators," Opt. Lett. **21**, 453–455 (1996).

8. A. Serpenguzel, S. Arnold, and G. Griffel, "Excitation of resonances of microspheres on an optical fiber," Opt. Lett. **20**, 654–656 (1995).

9. J. G. Knight, G. Cheung, F. Jacques, and T. A. Birks, "Phase-matched excitation of whispering-gallery-mode resonances by a fiber taper," Opt. Lett. **22**, 1129–1131 (1997).

10. S. Shibata, S. Ashida, H. Segawa, and T. Yano, "Coated microsphere as spherical cavity Raman laser," J. Sol-Gel Sci. Technol. **40**, 379–384 (2006).

11. S. Shibata, T. Yano, and H. Segawa, "Sol-gel-derived spheres for spherical microcavity," Acc. Chem. Res. **40**, 913–920 (2007).

12. S. Shibata, T. Yano, and H. Segawa, "Organic–inorganic hybrid materials for photonic applications," IEEE J. Sel. Top. Quantum Electron. **14**, 1361–1369 (2008).

13. H. Uehara, T. Yano, and S. Shibata, "Terrace formation with a picoliter sol-gel droplet for spherical cavity Raman laser," J. Sol-Gel Sci. Technol. **58**, 319–325 (2011).

14. H. Uehara, T. Yano, and S. Shibata, "Terrace-microsphere lasers: spherical cavity lasers for multi-wavelength emission," Proc. SPIE **7598**, 75981E (2010).

15. A. S. L. Gomes and N. M. Lawandy, "Efficient stimulated Raman scattering externally seeded by molecular spontaneous emission," Opt. Lett. **19**, 408–410 (1994).

16. A. F. Kwok and R. K. Chang, "Fluorescence seeding of weaker-gain Raman modes in microdroplets: enhancement of stimulated Raman scattering," Opt. Lett. **17**, 1262–1264 (1992).

17. J. Cheng, A. Y. S. Cheng, Y. He, H. Zuo, and J. Yang, "Enhancement of stimulated Raman scattering of CS_2 by using fluorescence of R6G," Opt. Commun. **246**, 141–145 (2005).

18. M. Saito, T. Yano, H. Segawa, and S. Shibata, "Site-selective excitation and fluorescence of Nd^{3+} ion-doped glasses for lasing at 900 nm band," presented at the 3rd International Conference on Science and Technology for Advanced Ceramics, Yokohama, Japan, June 16-18, 2009.

19. B. O. Mysen and P. Richet, "The titanium anomalies," in *Silicate Glasses and Melts* (Elsevier, 2005), pp. 357–386.

20. C. Schultz-Münzenberg, "The quasi-static structure of oxide glasses, in *Analysis of the Composition and Structure of Glass and Glass Ceramics*, H. Bach and D. Krause, eds. (Springer, 1999), pp. 141–311.

21. V. Sandoghdar, F. Treussart, J. Hare, V. Lefevre-Seguin, J. M. Raimond, and S. Haroche, "Very low threshold whispering-gallery-mode microsphere laser," Phys. Rev. A **54**, R1777 (1996).

22. M. Domenecha and G. Lifante, "Continuous-wave laser operation at $1.3\,\mu$m in Nd^{3+}-doped Zn:$LiNbO_3$ channel waveguides," Appl. Phys. Lett. **84**, 3271–3273 (2004).

23. X. Pu and Z. Yang, "Enhancement of stimulated Raman scattering of weak-gain Raman modes in a pendant drop by dye-lasing gain," J. Opt. Soc. Am. B **21**, 343–348 (2004).

24. R. Symes, H. Meresman, R. M. Sayer, and J. P. Reid, "A quantitative demonstration of the enhancement of cavity enhanced Raman scattering by broad band external laser seeding," Chem. Phys. Lett. **419**, 545–549 (2006).

25. S. Wada, H. Moriwaki, A. Nakamura, and H. Tashiro, "Injection seeding for the enhancement of high-order anti-Stokes stimulated Raman scattering," Opt. Lett. **20**, 848–850 (1995).

26. G. P. Agrawal, "Theory of Raman amplifiers," in *Raman Amplification in Fiber Optical Communication Systems*, C. Headley and G. P. Agrawal, eds. (Elsevier, 2005), pp. 33–102.

27. J. A. Dharmadhikari, A. K. Dharmadhikari, A. Mishra, and G. Ravindra Kumar, "Amplified spontaneous emission enhanced forward stimulated Raman scattering in dye solutions," Appl. Phys. B **76**, 755–759 (2003).

28. R. R. B. Correia, P. Alcantara, and S. L. S. Cunha, "Dye-induced spectral narrowing of stimulated scattering in CS_2," Chem. Phys. Lett. **313**, 553–558 (1999).